Growth of two-dimensional C60 nano clusters within a propylthiolate matrix

Gao, Jianzhi; Gao, Juyang; Yan, Chao; Rokni Fard, Mahroo; Kaya, Dogan; Zhu, Gangqiang; Guo, Quanmin

DOI:
10.1021/acs.jpcc.6b09259

Document Version
Peer reviewed version

Citation for published version (Harvard):
Gao, J, Gao, J, Yan, C, Rokni Fard, M, Kaya, D, Zhu, G & Guo, Q 2016, 'Growth of two-dimensional C60 nano clusters within a propylthiolate matrix', *Journal of Physical Chemistry C*, vol. 120, no. 44, pp. 25481–25488. https://doi.org/10.1021/acs.jpcc.6b09259

Growth of Two-Dimensional C_{60} Nano-Clusters Within a Propylthiolate Matrix

Jianzhi Gao[1], Juyang Gao[1], Chao Yan[1], Mahroo Rokni Fard[2], Dogan Kaya[2], Gangqiang Zhu[*1] and Quanmin Guo*[2]

[1] *School of Physics and Information Technology, Shaanxi Normal University, Xi'an 710119, China*

[2]*School of Physics and Astronomy, University of Birmingham, Birmingham B15 2TT, United Kingdom*

ABSTRACT

Two-dimensional C_{60} clusters embedded in a propylthiolate/Au(111) self-assembled monolayer (SAM) are produced by depositing C_{60} molecules on top of the SAM at 110 K followed by thermal annealing to room temperature. The SAM acts as a spacer layer at 110 K preventing C_{60} molecules from reaching the Au(111) substrate. As temperature is increased, molecular scale vacancies open up within the SAM allowing C_{60} molecules to drop to the surface of the Au(111) substrate. This initial "rooting" is then followed by the formation of two-dimensional C_{60} clusters. The clusters have a rather uniform orientation with a well-defined direction for the close-packed C_{60} molecules.

* Corresponding authors, email: zgq2006@snnu.edu.cn. Tel: +86 2981530750. Q.guo@bham.ac.uk. Tel: +44 1214144657.

Introduction

Self-assembly of molecular structures represents one of the most promising and practical routes for bottom-up nanotechnology.[1] During the last decade, there has been a rapid growing interest in transferring supramolecular self-assembly to solid surfaces[2-4] for a number of reasons. First of all, there is the technological demand for anchoring molecular structures on a substrate for the purpose of device fabrication. Secondly, in terms of fundamental studies, there are a large number of characterization techniques particularly suitable for analysing molecules attached to solid surfaces. Among them are scanning tunnelling microscopy (STM) and atomic force microscopy (AFM), both capable of imaging molecules with atomic resolution and hence providing direct information on bonding mechanisms.[2,3] Moreover, the solid surface itself plays a role in the assembly process, offering the opportunity to build molecular architectures that are not viable in liquid environment.

Assembly of molecular structures on solid surfaces is based mostly on the same 3-D non-covalent bonding mechanism as in solutions. The building blocks are linked together by either hydrogen bonding [5-10] or through metal-ligand coordination.[11-16] The effects of dipolar interaction [17, 18] and the van der Waals (vdW) interaction have also been investigated.[19, 20] Hydrogen bonding and metal-ligand coordination share the common feature that bonding is directional and occurs specifically in between the relevant functional groups. The localized nature of directional bonding is responsible for the formation of many interesting porous molecular networks.[2, 6, 10, 21] For molecules where van der Waals force is the dominant force for bonding, the choice of structures that can be achieved becomes very limited because vdW force tends to drive the molecules into a non-characteristic close-packed arrangement. Therefore, molecular assembly based purely on vdW forces is less controllable. The delocalized nature of the vdW forces and consequently the lack of directional bonding involving such forces create a substantial obstacle in both experimental characterization and theoretical simulation of vdW bonded systems. However, a unique property of the vdW force is that it scales with the size of the molecule and is thus expected to play a dominant role in assembly of large molecules, in particular molecules that are important to living

organisms and life.

C_{60} does not have specific functional groups and the interaction among the molecules is mainly van der Waals in character. As a result, C_{60} molecules tend to form close-packed layers on the less reactive (111) plane of many fcc metals [22-34] including gold.[35-48] Step edges are the usual sites for nucleation at room temperature and the resulting C_{60} layer can expand to cover the entire atomic terrace. In order to form nanometer-sized C_{60} clusters, one needs to introduce a mechanism to suppress the formation of large extended structures. On the Au(111) surface, small clusters can be formed at the elbow sites on the herringbone-reconstructed Au(111) at low sample temperatures.[47] However, these clusters are not stable at room temperature. Here we report the formation of nanometer-sized two-dimensional C_{60} clusters embedded within a propylthiolate monolayer on Au(111). Depending on the surface pressure, the propylthiolate monolayer can exist in a range of structural phases from the most dense (3×4) to a number of lower density striped phases.[49-51] We deposit C_{60} molecules onto a striped propylthiolate layer with 0.22 ML coverage. The presence of propylthiolate on Au(111) has been found to have a significant effect on both the diffusion of individual C_{60} molecules and the growth of C_{60} clusters.

Experimental Section

The Au(111) sample is a thin film (~300 nm) deposited on a highly oriented pyrolitic graphite (HOPG) substrate using thermal evaporation in a BOC Edwards Auto 306 deposition system. The sample, after transferring into the ultra-high vacuum STM chamber, is cleaned with Ar+ ion bombardment and thermal annealing. The sample is then exposed to CH_3-S-S-$(CH_2)_2$-CH_3 vapor at RT to form a 0.33 ML mixed thiolate layer consisting of CH_3-S-Au-S-$(CH_2)_2$-CH_3, CH_3-S-Au-S-CH_3, and CH_3-$(CH_2)_2$-S-Au-S-$(CH_2)_2$-CH_3. By heating up the sample to 420 K, CH_3-S is removed from the surface via thermal desorption of CH_3-S–S-CH_3. The remaining CH_3-$(CH_2)_2$-S-Au-S-$(CH_2)_2$-CH_3 re-organize into the striped phase.

C_{60} molecules are deposited onto the propyl-thiolate covered gold sample at 110 K from a home-made Knudsen cell in the form of a tantalum pocket with a pinhole

aperture. The Ta cell is heated resistively with its temperature measured by a K-type thermocouple. The rate of deposition is approximately 0.1 ML/min at a cell temperature of 706 K, as estimated from the C_{60} coverage measured with the STM. Imaging was performed using an Omicron variable temperature STM (VT-STM) with electrochemically etched tungsten tips.

Results and Discussion

Figure 1a shows an STM image of a propylthiolate layer in its $(3\sqrt{3} \times \sqrt{3})$-R30° phase. The basic feature of this propylthiolate layer is parallel rows aligned in the $[11\bar{2}]$ and other two equivalent directions. Each row consists of CH_3-$(CH_2)_2$-S-Au-S-$(CH_2)_2$-CH_3 units as shown in Figure 1b.[50] In the following, we will refer CH_3-$(CH_2)_2$-S-Au-S-$(CH_2)_2$-CH_3 as $(C_3S)_2$-Au for simplicity. In high-resolution STM images, each $(C_3S)_2$-Au unit is seen as two protrusions, one from each CH_3 group.[51] The distance between two adjacent rows is 4.5*a* (1.3 nm) where *a* is the distance between nearest neighbor gold atoms. The coverage is 0.22 ML of S-$(CH_2)_2$-CH_3. The maximum coverage can be achieved is 0.33 ML of S-$(CH_2)_2$-CH_3 corresponding to the formation of the (3 × 4) phase.[50] Here the coverage is defined, following the existing convention, as the number of (C_3S) per surface Au atom. 0.33 ML hence corresponds to the situation that Au(111) is unable to accommodate any extra molecules. In addition to the $(3\sqrt{3} \times \sqrt{3})$-R30° phase shown in Fig. 1, there are a number of the so-called striped phases that can form on the Au(111) surface.[49] Each striped phase consists of regularly spaced $(C_3S)_2$-Au rows. The distance between neighboring two rows is coverage dependent.[49, 52, 53] One striped phase can change into another when the molecular coverage changes. Also shown in Fig. 1a, highlighted with a yellow circle, is a boundary region between rotational $(3\sqrt{3} \times \sqrt{3})$-R30° domains. Short $(C_3S)_2$-Au rows oriented in all three equivalent directions are formed inside the boundary. As a result, the packing density within the boundary is lower than 0.22 ML.

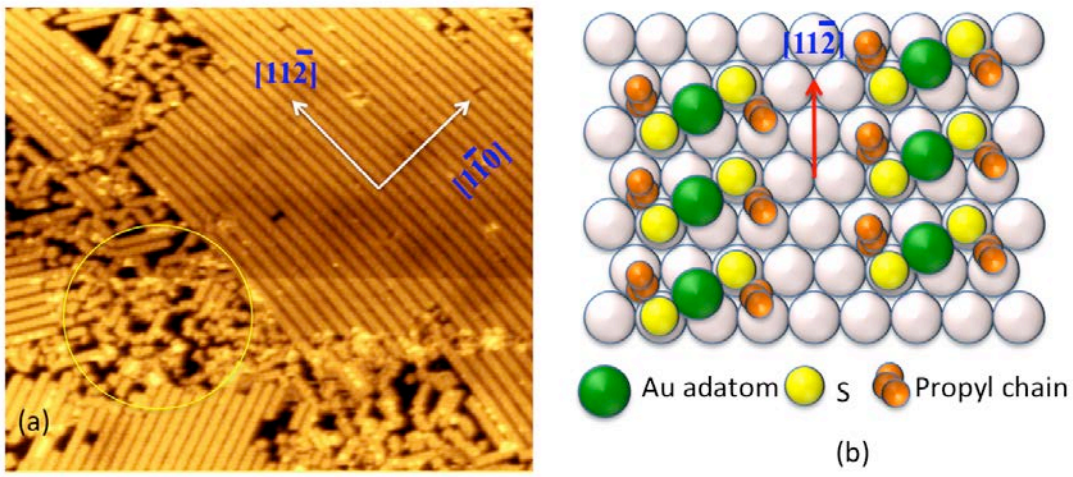

Figure 1. (a) STM image, 65 nm × 57 nm, obtained using –1.14 V sample bias and 0.15 nA tunneling current at RT from Au(111) with 0.22 ML of propylthiolate. Lack of order is observed within boundaries between rotational domains. (b) Structural model showing the $(C_3S)_2$-Au rows aligned in the $[11\bar{2}]$ direction.

The Au sample covered by the $(3\sqrt{3} \times \sqrt{3})$-R30^o phase of propylthiolate is cooled down to 110 K at which point about 0.5 ML of C_{60} molecules are deposited. 1 ML of C_{60} is defined, in a more intuitive manner, as a single layer of closed-packed molecules on Au(111). This is different from the ML definition used for the propylthiolate SAM in which case we have to follow the convention so comparison to previous works can be made without confusion. If we were to use the same definition of the ML as for the thiolate, then a single layer of C_{60} on Au(111) would become 1/12 ML. C_{60} molecules are found to form several different structures as shown in Figure 2. One type of structures is in the form of C_{60} molecular rows aligned along the $[11\bar{2}]$ direction. The distance between neighboring molecules along the row is 1 ± 0.05 nm, hence molecules are close-packed along the row. The distance between two adjacent C_{60} rows, rows inside the blue rectangle for example, matches the period of the $(C_3S)_2$-Au stripes. These C_{60} rows are found to be located in between two $(C_3S)_2$-Au rows as illustrated in Fig. 2b. A schematic diagram showing the relative position of the C_{60} molecule is given in Figure 3. In addition to the molecular rows, patches of C_{60} islands exhibiting two-dimensional close-packed feature are also observed. The three red circles in Fig. 2a highlight the formation of such close-packed islands. From the above observations, we

can conclude that the thiolate rows have the ability to confine the C_{60} molecule, but the confinement is not strong enough to stop C_{60} molecules from joining into close-packed islands at 110 K.

Inset in Fig. 2a is a height profile acquired along line A-B in the image. The molecules appear 0.95 ± 0.02 nm above the SAM. At the boundary between rotational domains, region highlighted by yellow circle in Fig. 1 for example, $(C_3S)_2$-Au are less well organized. In such areas, C_{60} molecules do not seem to form any ordered structure as shown in Fig. 2c. However, in terms of height, the molecules can easily be separated into two groups. The "bright" molecules in Fig. 2c appear ~ 1nm above the SAM, whereas the "dim" molecules appear 0.70 ± 0.02 nm tall. As can be seen in Fig. 1a, the density of the propylthiolate is low at the domain boundaries and there appear large gaps in between some $(C_3S)_2$-Au rows. It is thus possible that C_{60} molecules inside the domain boundaries can drop all the way down and make contact with the Au(111) substrate. Therefore, the dim molecules are likely to be in direct contact with the Au(111) substrate, and the bright molecules are decoupled from the substrate by $(C_3S)_2$-Au. Since molecules in Fig. 2a appear 0.95 ± 0.02 nm tall, they are also decoupled from the substrate. According to the schematic shown in Fig. 3, the propyl chains occupy the space between the C_{60} molecule and the Au(111) substrate preventing direct C_{60}-Au contact.

Data presented in Fig. 2 suggest that when C_{60} molecules land on the surface at 110 K, they diffuse rather freely along the $[11\bar{2}]$ direction and form single-molecule-wide rows. The formation of C_{60} rows is similar to that reported by Zeng *et al* in their study of C_{60} adsorption on a decanethiol monolayer.[54] The C_{60} row is located in between two $(C_3S)_2$-Au rows and are prevented from contacting the Au(111) substrate by the protruding propyl chains. The spacing between two neighboring C_{60} rows is thus the same as that between two $(C_3S)_2$-Au rows. However, the interaction between C_{60} and $(C_3S)_2$-Au is rather weak allowing the attractive interaction between C_{60} molecules to bring the C_{60} rows closer together and form two-dimensionally close-packed C_{60} islands in certain places. In such places, the $(C_3S)_2$-Au layer becomes sandwiched

between Au(111) and the closed-packed C_{60} islands. Only in places where large enough bare Au(111) surface is exposed, can C_{60} molecules adsorb directly on Au(111).

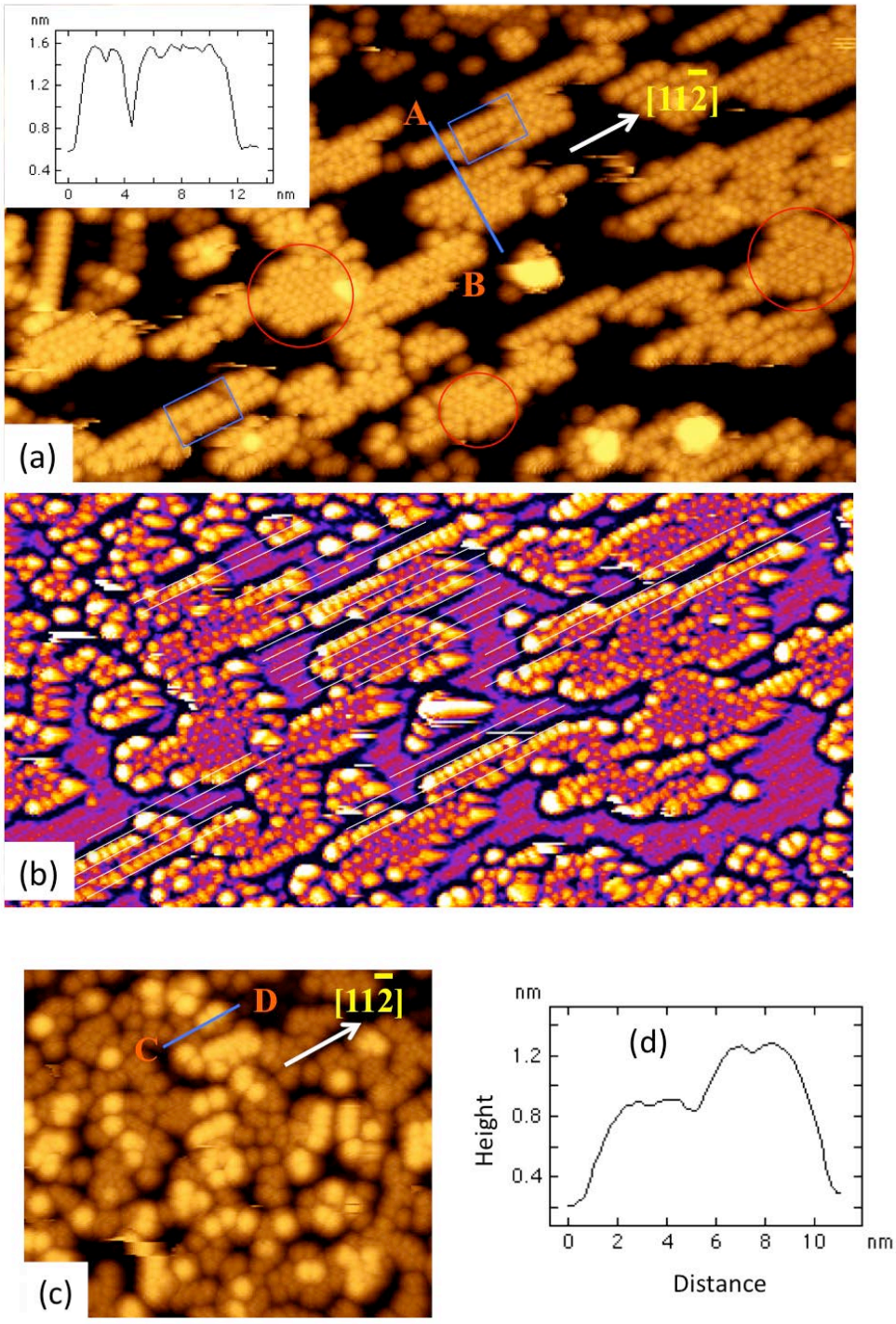

Figure 2. (a) STM image, 82 nm × 46 nm, obtained using –2.14 V sample bias and 0.03 nA tunneling current at 110 K from Au(111) with 0.5 ML of C_{60} deposited on top of 0.22 ML of propylthiolate. Inset shows a height profile taken along line A-B. (b) Filtered STM image used to determine the position of the C_{60} rows relative to that of the propylthiolate rows. The straight lines indicate the $(C_3S)_2$-Au rows. (c) STM image, 49 nm × 42 nm, obtained using –2.14 V sample bias

and 0.03 nA tunneling current, of C_{60} molecules inside the domain boundaries of the SAM. (d) Height profile acquired across line C-D in (c) shows that the “bright” molecules appear taller than the “dim” molecules by ~0.3 nm.

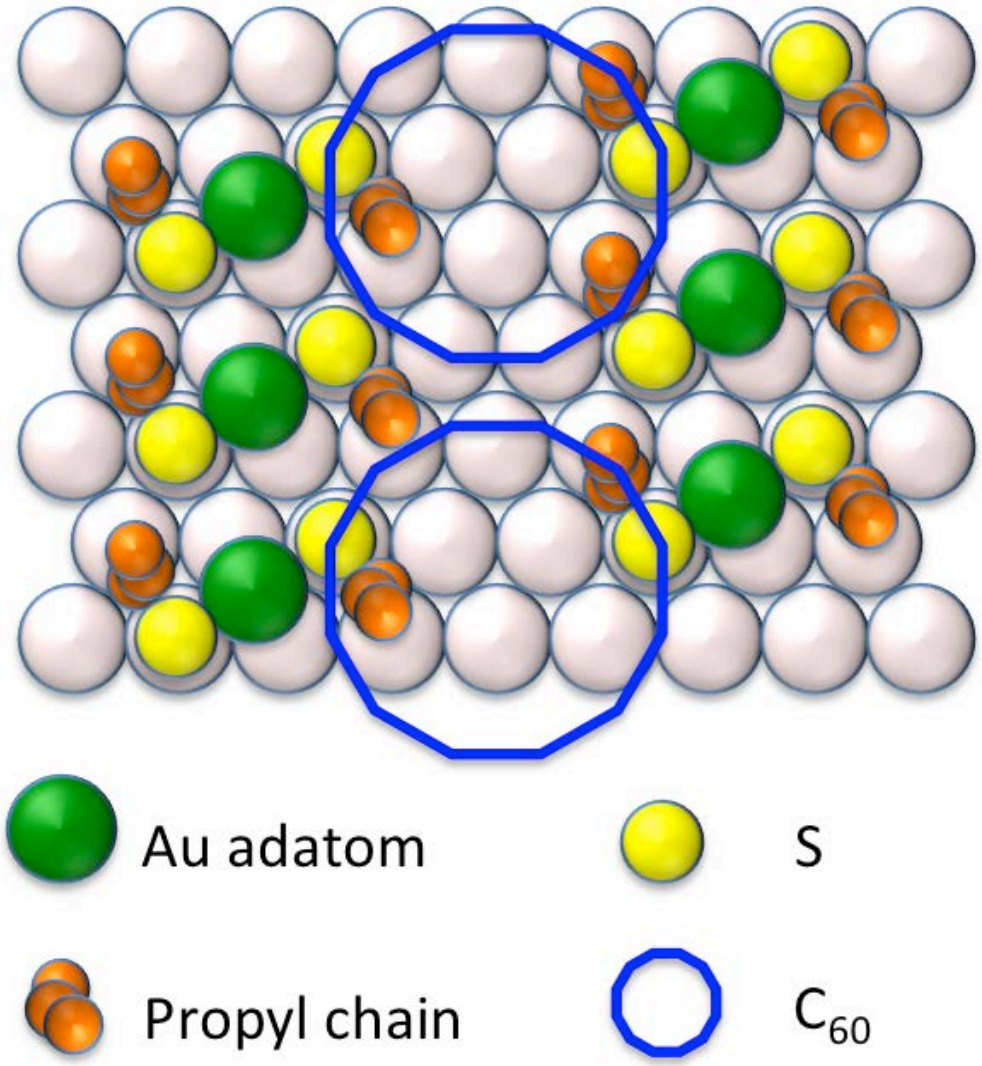

Figure 3. Ball model illustrating the location of C_{60} molecules between two $(C_3S)_2$-Au rows.

Warming the C_{60}/ $(C_3S)_2$-Au/Au(111) sample to room temperature brings drastic changes to the surface morphology. The C_{60} molecules, floating on top of the SAM at 110 K, have all moved down to make direct contact with the Au(111) substrate. Figure 4a shows an STM image of the sample acquired at RT over a relatively large area of 500 nm × 500 nm. A large number of close-packed C_{60} clusters have appeared. These clusters consist of closed-packed molecules with regular shapes as shown in the

high-resolution image of Figure 4b. Inset in Fig. 4b shows that the C_{60} clusters are 0.6 nm tall. This is similar to the height of the dim C_{60} molecules in Fig. 2c. Thus, we can conclude that C_{60} clusters in Fig. 4 sit directly above the Au(111) substrate with the space in between the islands filled by the SAM. With half of the Au(111) surface now overtaken by C_{60} molecules, the $(C_3S)_2$-Au layer is expected to be in its highest density phase which is known as the 3 × 4 phase.[50] The 3 × 4 phase can be clearly imaged with the STM at RT.[50] However, the space-filling SAM as shown in Fig. 4b appears to have no ordered structure. Based on a simple evaluation of the fractional surface area occupied by the SAM, the density of $(C_3S)_2$-Au would have reached to a level well above the maximum density that can be reached on Au(111) in the absence of C_{60}. The maximum coverage of alkanethiol monolayers on Au(111) is 1/3 ML when there are no other co-adsorbed molecules. In the presence of C_{60}, it is not clear if the C_{60} molecules are able to compress the SAM even further. There is the possibility that compression may have caused partial desorption of thiolate as $(C_3S)_2$, although we do not have mass spectroscopy to measure desorption products. However, RT desorption of $(C_3S)_2$ is rather unusual. Even for methylthiolate monolayer on Au(111), thermal desorption is observed only when temperature reaches ~ 310 K.[52] Previous works with alkanthiol SAMs show that starting from a low coverage striped phase, adding more thiol molecules at RT results in compressing the SAM into ultimately the most dense phase at 0.33 ML coverage.[55] With C_{60} molecules competing for the same Au(111) surface, we expect that when C_{60} molecules drop down from above the propylthiolate layer to the gold substrate, the propylthiolate layer gets compressed into a higher density phase. No ordered structure is observed for areas in between the C_{60} clusters. It is noted that ordered structure for the striped phase shown in Fig. 1a as well as that for the 3 × 4 phase of propylthiolate[50] can be readily observed at RT. The absence of ordering seen for areas in between the C_{60} islands is hence a genuine effect. The initial regular striped phase is replaced by a disordered phase once C_{60} is incorporated into the thiolate matrix. Unfortunately, we are not able to give any further details of this disordered phase of propylthiolate without further studies. It is known that C_{60} withdraws charge from Au(111). This charge transfer may contribute to the weakening of the bonding between

propylthiolate and the Au(111) substrate. There is no preferential decoration of surface steps by C_{60} molecules as can be seen in Fig. 4a and b. This is because propylthiolate species at step edges are more strongly bound and thus more difficult to be replaced by C_{60}. The presence of propylthiolate has completely altered the growth mode of C_{60} on Au(111) allowing nucleation and growth only at locations away from the steps. In Fig. 4, one can see that most of the C_{60} clusters have molecules close-packed along the $[11\bar{2}]$ direction. A small fraction of the clusters have the molecules close-packed along the $[1\,\bar{1}0]$direction. These two close-packing directions are consistent with previous observations when only C_{60} molecules are present on the Au(111) surface.[27, 38, 44] However, in the presence of the propylthiol SAM, the fraction of $[11\bar{2}]$oriented clusters is significantly higher.

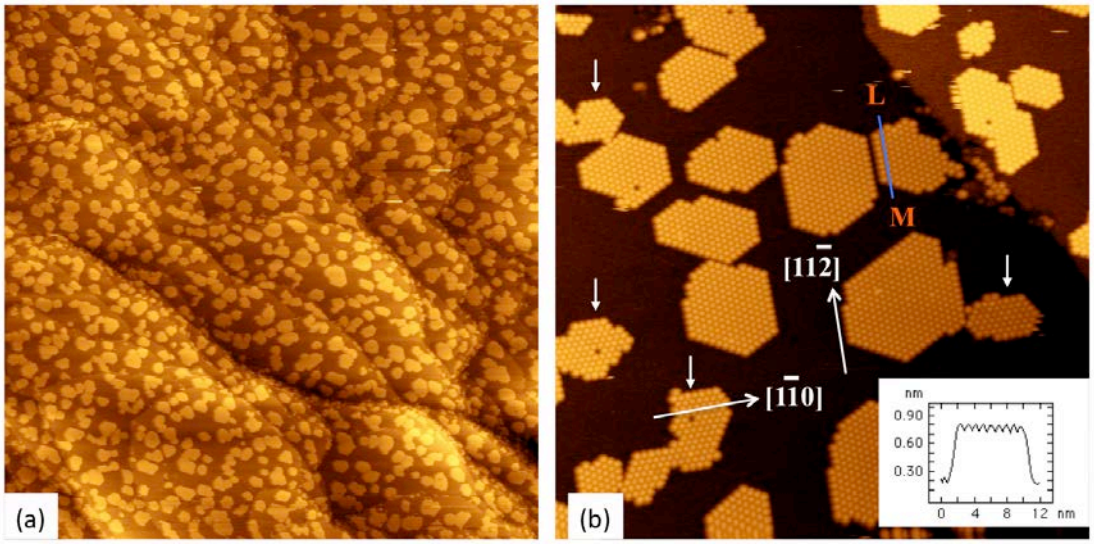

Figure 4. (a) STM image, 500 nm × 500 nm, obtained using –2.46 V sample bias and 0.04 nA tunneling current at RT from Au(111). (b) Zoomed-in image, 80 nm × 80 nm, acquired using –1.78 V sample bias and 0.03 nA tunnel current, showing the shape of the C_{60} islands. The majority of the clusters have the same orientation with $[11\bar{2}]$ the close-packing direction for C_{60} molecules. White arrows point to islands with the alternative orientation where C_{60} molecules are close-packed along the $[1\,\bar{1}0]$ direction. Inset shows a height profile plotted along line L-M.

The main steps in the formation of C_{60} clusters inside the SAM is further illustrated schematically in Figure 5. A vacancy in the SAM provides the initial anchoring point for the first C_{60} molecule. More molecules join in subsequently to form a cluster as the

SAM is ~~compressed and~~ pushed sideways. Further expansion of the C_{60} cluster becomes gradually more difficult when the density of the SAM around the C_{60} cluster approaches its maximal value. Nucleation and growth is still possible at other locations where the density of the SAM is low because the low coverage striped phase can exist side-by-side with the high coverage phase [49, 53,] The density of the SAM surrounding a large C_{60} cluster is expected to be higher than that around a smaller cluster. This leads to a decrease in the growth rate as the C_{60} cluster size increases and hence prevents the formation of very large clusters. In the presence of the thiolate monolayer, steps are no longer the preferred nucleation sites for C_{60} clusters.[56] Propylthiolate are so strongly bound to step edges that they cannot be displaced by C_{60} molecules. This is in great contrast with the formation of C_{60} clusters on bare Au(111) substrates where growth from step edges are always preferred.[27, 38, 46] Because of the existence of steps with different azimuthal orientations, on clean Au(111) surface, C_{60} molecules forms several domains of different orientations. By preventing nucleation from steps, all C_{60} clusters formed within the SAM matrix tend to have their close-packed molecular rows aligned with the $[11\bar{2}]$ direction.

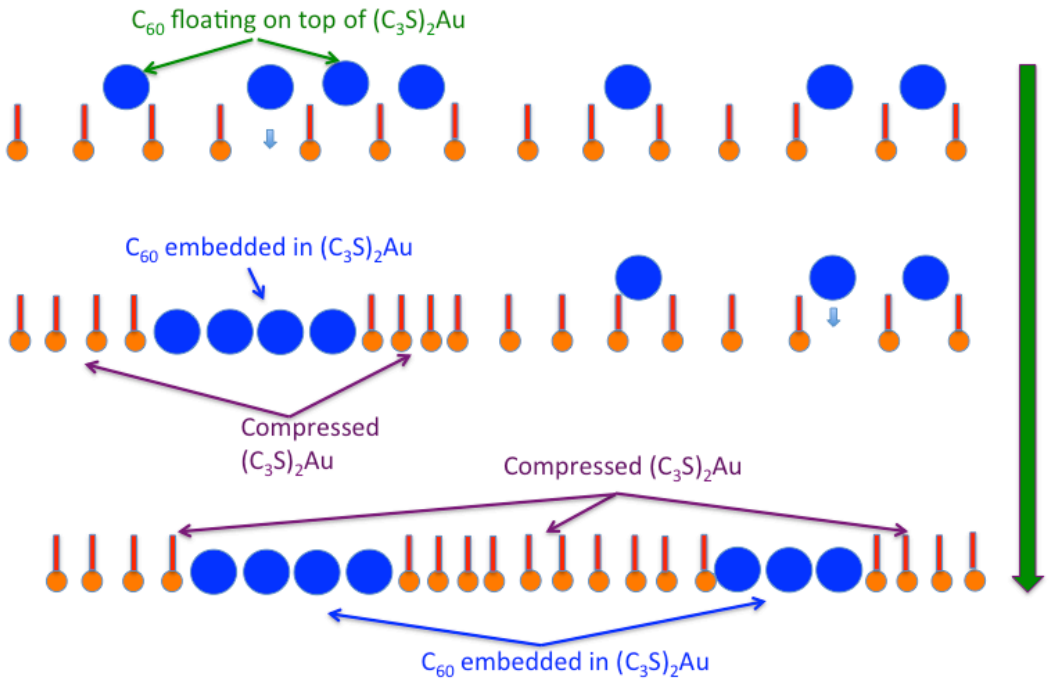

Figure 5. Illustration of the proposed mechanism showing how C_{60} molecules squeeze into the SAM as the temperature is raised. Green arrow at the right indicates the direction of increasing T. Formation of the C_{60} cluster compresses the SAM in the vicinity of the cluster. This leads to higher resistance against further growth of the cluster.

We next describe molecular exchange between neighboring C_{60} clusters. The molecular clusters as shown in Fig. 4a and b appear stable at room temperature. However, slow exchange of molecules between clusters is observed to occur on a relatively slow time scale. Figure 6 shows a series of images of a C_{60} cluster, collected over 10 minutes' time. Between two adjacent frames, we sometimes observe the number of molecules within the cluster to change by about ±3 molecules or ~2%. Over a long period of time, there is no gross growth of one cluster at the expense of others such as that predicted by Ostwald ripening. Each cluster is stable with the number of molecules remaining rather

constant subject to minor fluctuations. The presence of the propylthiolate SAM, in particular the high coverage phase of the SAM, suppresses the diffusional movement of C_{60} molecules between C_{60} clusters.

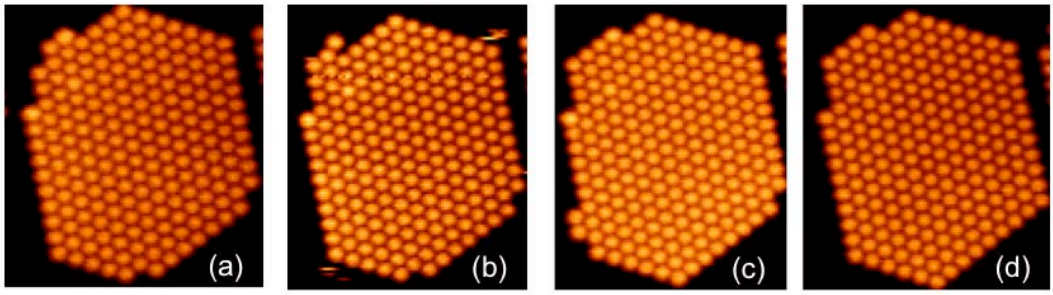

Figure 6. STM images taken sequentially from a C_{60} cluster over 10 minutes' time at room temperature.

The size distribution of C_{60} clusters formed at RT within the SAM is plotted and shown in Figure 7a. The average cluster consists of 130 C_{60} molecules. In contrast, when depositing on a bare Au(111) surface at RT, C_{60} molecules form very large islands only limited by the size of the atomic terrace of the Au(111) substrate.[27, 38] Figure 7b shows how the number of molecules in typical C_{60} clusters fluctuates with time at room temperature. We have randomly chosen three clusters from a large number of clusters and monitored their sizes as a function of time.

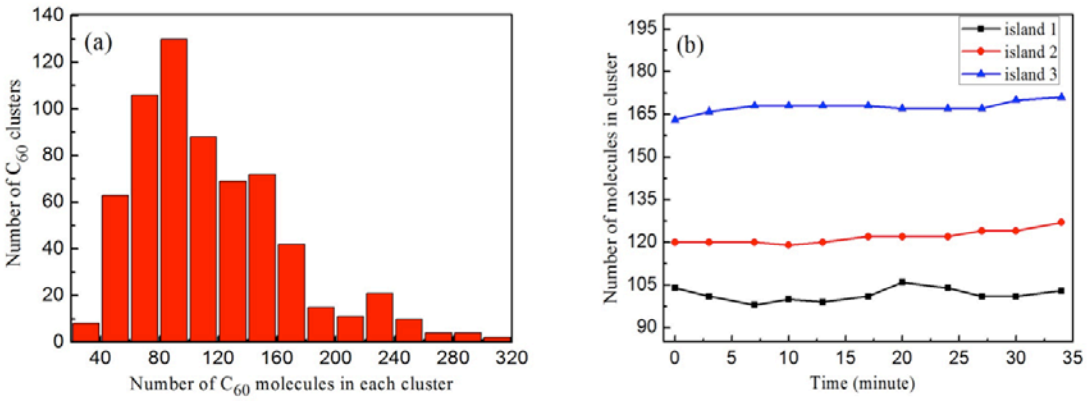

Figure 7. (a) Size distribution of C_{60} clusters based on the measurement from a total number of 645 clusters. The average cluster consists of 130 molecules. (b) The number of molecules within the C_{60} cluster measured as a function of time at RT. Three clusters of different sizes are followed over 35 minutes.

The effect of the propylthiolate monolayer on the growth of C_{60} clusters can be demonstrated further by comparing the behavior of C_{60} on the clean Au(111) surface. Fig. 8a shows an STM image where C_{60} clusters can be seen to have formed at the elbow sites at 45 K. When the sample is subsequently warmed up to RT, mass migration of the molecules to step edges takes place as shown in Fig. 8b. Disintegration of the clusters is found when temperature reaches to ~ 200 K. Therefore, in the absence of the thiolate monolayer, the small C_{60} clusters are much less stable. When C_{60} molecules are deposited onto Au(111) at RT, very large C_{60} islands are formed. The coverage of C_{60} shown in Fig. 8c is comparable to that in Fig. 4a.

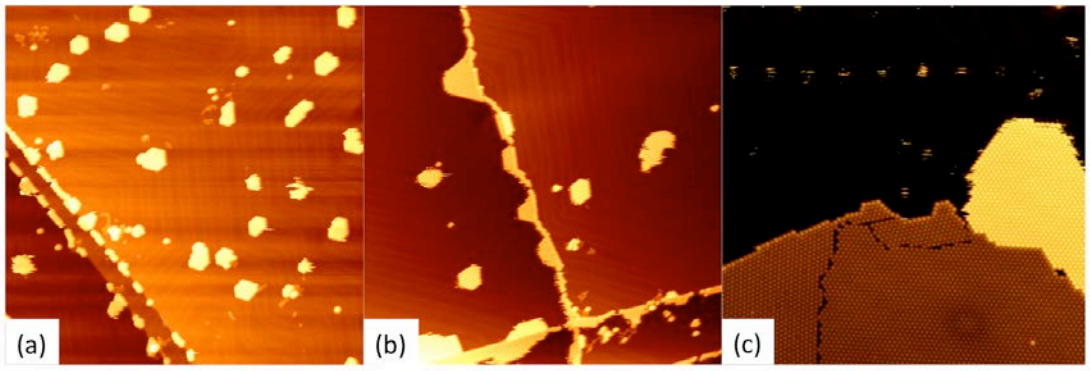

Figure 8. (a) and (b). STM images, 120 nm × 120 nm obtained using –1.45 V bias voltage and 0.01 nA tunnel current, showing the behavior of C_{60} molecules sitting on the clean surface of Au(111). (a) C_{60} molecules form molecular clusters at the elbow sites. (b) Upon warming to RT, most clusters disappear from the elbow sites. C_{60} molecules are found to aggregate along step edges. (c) Large C_{60} islands are formed when C_{60} molecules are deposited onto Au(111) at RT.

There have been a number of studies involving the organization of C_{60} molecules assisted by the co-adsorption of another molecule by exploiting the interaction of C_{60} with the co-adsorbate.[57-64] For instance, a well known scheme is to mix C_{60} molecules with an electropositive molecule so that charge transfer between the molecules leads to the stabilization of a donor-acceptor configuration.[57] Donor-acceptor interaction leads to the formation of regular molecular networks, similar to the formation of supramolecular networks using hydrogen bonding [5-10] or metal-organic coordination. [11-16] Our system consists of two electronegative species, C_{60} and propylthiolate, competing for charge from the metal substrate. Separate phases of C_{60} and thiolate SAM are formed. In an earlier study of the co-adsorption of C_{70} and octanethiol on Au(111) by Deering and Kandel,[64] it was found that pre-adsorbed C_{70} molecules were

pushed aside when octanethiol molecules were added to the substrate. The possibility of the propylthiolate SAM to exist in many coverage dependent structural phases makes the SAM a compressible matrix that can regulate the growth of C_{60} clusters.

Conclusions

To summarize, we have demonstrated that small C_{60} clusters can be formed within a propylthiolate matrix. C_{60} clusters consist of close-packed C_{60} molecules with well-defined azimuthal orientations. The propylthiolate offers resistance against the diffusion C_{60} molecules and hence hinders the formation of large clusters via the usual Ostwald ripening process.

Acknowledgements

This work was supported by the National Science Foundation of China (Grant no. 11604196) and Fundamental Research Funds for the Central Universities (Grant no. GK201602008 and GK201603013).

References

[1] Chakrabarty, R.; Mukherjee, P. S.; Stang. P. J. Supramolecular coordination: Self-assembly of finite two- and three-dimensional ensembles. *Chem. Rev*. **2011**, *111*, 6810-6818.

[2] Barth. J. V. Molecular architectonic on metal surfaces. *Annu. Rev. Phys. Chem*. **2007**, *58*, 375-407.

[3] Elemans, J. A. A. W.; Lei, S. B.; De Feyter, S. Molecular and supramolecular networks on surfaces: From two-dimensional crystal engineering to reactivity. *Angew. Chem. Int. Ed*. 2**009**, *48*, 7298-7332.

[4] Rosei, F.; Schnack, M.; Naitosh, Y.; Jiang, P.; Gourdon, A.; Lagsgaard, E.; Stensgaard, I.; Joachim, C.; Besenbacher, F. Properties of large organic molecules on metal surfaces. *Prog. Surf. Sci*. **2003**, *71*, 95-146.

[5] Dmitriev, A.; Lin, N.; Weckesser, J.; Barth, J. V.; Kern, K. Supramolecular assemblies of

trimesic acid on a Cu(100) surface. *J. Phys. Chem. B*. **2002**, *106*, 6907-6912.

[6] Theobald, J. A.; Oxtoby, N. S.; Phillips, M. A.; Champness, N. R.; Beton. P. H. Controlling molecular deposition and layer structure with supramolecular surface assemblies. *Nature*. 2**003**, *424*, 1029-1031.

[7] Ciesielski, A.; Szabelski, P. J.; Rzysko, W.; Cadeddu, A.; Cook, T. R.; Stang P. J.; Samori. P. Concentration-dependent supramolecular engineering of hydrogen-bonded nanostructures at surfaces: Predicting self-assembly in 2D. *J. Am. Chem. Soc*. **2013**, *135*, 6942-6590.

[8] Fendt, L. A.; Stohr, M.; Wintjes, N.; Enache, M.; Jung T. A.; Diederich. F. Modification of supramolecular binding motifs induced by substrate registry: Formation of self-assembled macrocycles and chain-like patterns. *Chem. Eur. J*. **2009**, *15*, 11139-11150.

[9] Jewell, A. D.; Simpson, S. M.; Enders, A.; Zurek, E.; Sykes, E. C. H. Magic electret clusters of 4-fluorostyrene on metal surfaces. *J. Phys. Chem. Lett*. **2012**, *3*, 2069-2075.

[10] Pawin, G.; Wong, K. L.; Kwon, K. Y.; Bartels, L. A homomolecular porous network at a Cu(111) surface. *Science* **2006**, *313*, 961-962.

[11] Pivetta, M.; Pacchioni, G. E.; Schlickum, U.; Barth, J. V.; Brune, H. Formation of Fe cluster superlattice in a metal-organic quantum-box network. *Phys. Rev. Lett*. **2013**, *110*, 086102.

[12] Yang, H. H.; Chu, Y. H.; Lu, C. I.; Yang, T. H.; Yang, K. J.; Kaun, C. C.; Hoffmann, G. Lin, M. T. Digitized charge transfer magnitude determined by metal-organic coordination number. *ACS Nano*. **2013**, *7*, 2814-2819.

[13] Mendez, J.; Caillard, R.; Otero, G.; Nicoara, N.; Martin-Gago, J. A. Nanostructured organic material: From molecular chains to organic nanodots. *Adv. Mater*. **2006**, *18*, 2048.

[14] Hanke, F.; Haq, S.; Raval, R.; Persson, M. Heat-to-connect: Surface commensurability directs organometallic one-dimensional self-assembly. *ACS Nano.* **2011**, *5*, 9093-9103.

[15] Klappenberger, F.; Kuhne, D.; Krenner, W.; Silanes, I.; Arnau, A.; Garcia De Abajo, F. J.; Klyatskaya, S.; Ruben, M.; Barth, J. V. Tunable quantum dot arrays formed from self-assembled metal-organic networks. *Phys. Rev. Lett*. 2**011**, *106*, 026802.

[16] Ecija, D.; Urgel, J. I.; Papageorgiu, A. C.; Joshi, S.; Auwarter, W.; Seitsonen, A. P.; Klyatskaya, S.; Ruben, M.; Fischer, S.; Vijayaraghavan, S.; Reichert, J.; Barth, J. V. Five-vertex Archimedean surface tessellation by lanthanide-directed molecular self-assembly. *PNAS*. **2013**, *110*, 6678-6681.

[17] Bischoff, F.; Seufert, K.; Auwarter, W.; Joshi, S.; Vijayaraghavan, S.; Ecija, D.; Diller, K.;

Papageorgiu, A. C.; Fischer, S.; Allegretti, F.; Ducan, D. A.; Klappenbeger, F.; Blobner, F.; Han, R.; Barth, J. V. How surface bonding and repulsive interactions cause phase transformations: Ordering of a prototype macrocyclic compound on Ag(111). *ACS Nano*. **2013**, *7*, 3139-3149.

[18] Fernandez-Torrente, I.; Monturet, S.; Franke, K. J.; Fraxedas, J.; Lorente, N.; Pascual, J. I. Long-range repulsive interaction between molecules on a metal surface induced by charge transfer. *Phys. Rev. Let*. **2007**, *99*, 176103.

[19] Chen, T.; Pan, G. B.; Wettach, H.; Fritzsche, M.; Hoger, S.; Wan, L. J.; Yang, H. B.; Northrop, B. H.; Stang, P. J. 2D assembly of metallacycles on HOPG by shape-persistent macrocycle templates *J. Am. Chem. Soc.* **2010**, *132*, 1328-1333.

[20] De Boer, D.; Krikorian, M.; Esser, B.; Swager, T. M. STM study of gold(I) pyrazolates: Distinct morphologies, layer evolution, and cooperative dynamics. *J. Phys. Chem. C.* **2013**, *117*, 8290-8298.

[21] Zhang, C.; Xie, L.; Wang, L.; Kong, H.; Tan, Q.; Xu, W. Atomic-scale insight into tautomeric recognition, separation, and interconversion of Guanine molecular networks on Au(111). J. *Am. Chem. Soc*. **2015**, 137, 11795-11800.

[22] Sau, J. D.; Neaton, J. B.; Choi, H. J.; Louie, S. G.; Cohen, M. L. Electronic energy levels of weakly coupled nanostructures: C-60-metal interfaces. *Phys. Rev. Lett.* **2008**, *101*, 026804.

[23] Larsson, J. A.; Elliott, S. D.; Greer, J. C.; Repp, J.; Meyer, G.; Allenspach, R. Orientation of individual C-60 molecules adsorbed on Cu(111): Low-temperature scanning tunneling microscopy and density functional calculations. *Phys. Rev. B.* **2008**, **7***7*, 115434.

[24] Guo, S.; Fogarty, D. P.; Nagel, P. M.; Kandel, S. A. Thermal diffusion of C-60 molecules and clusters on Au(111) *J. Phys. Chem. B*. **2004**, *108*, 14074-14081.

[25] Murray, P. W.; Pedersen, M. O.; Laegsgaard, E.; Stensgaard, I.; Besenbacher, F. Growth of C-60 on Cu(110) and Ni(110) surfaces: C-60-induced interfacial roughening. *Phys. Rev. B*. **1997**, *55*, 9360-9363.

[26] Weckesser, J.; Cepek, C.; Fasel, R.; Barth, J. V.; Baumberger, F.; Greber, T.; Kern, K. Binding and ordering of C-60 on Pd(110): Investigations at the local and mesoscopic scale. *J. Chem. Phys.* **2001**, *115*, 9001-9009.

[27] Altman, E. I.; Colton, R. J. Determination of the orientation of C-60 adsorbed on Au(111) and Ag(111) . *Phys. Rev. B.* **1993**, *48*, 18244-18249.

[28] Pai, W.; Hsu, C. L. Ordering of an incommensurate molecular layer with adsorbate-induced reconstruction: C-60/Ag(100). *Phys. Rev. B.* **2003**, *68*, 121403.

[29] Li, H. I.; Franke, K. J.; Pascual, J. I.; Bruch, L. W.; Diehl, R. D. Origin of Moireacute structures in C-60 on Pb(111) and their effect on molecular energy levels. *Phys. Rev. B.* 2**009**, *80*, 085415.

[30] Rowe, J. E.; Rudolf, P.; Tjeng, L. H.; Malic, R. A.; Meigs, G.; Chen, C. T.; Chen, J.; Plummer, E. W. Synchrotron radiation and low-energy-electron-diffraction studies of ultra thin C-60 films deposited on Cu(100), Cu(111) and Cu(110). *Int. J. Mod. Phys. B.* **1992**, *6*, 3909-3913.

[31] Altman, E. I.; Colton, R. J. The interaction of C-60 with noble-metal surfaces. *Surf. Sci.* **1993**, *295*, 13-33.

[32] Felici, R.; Pedio, M.; Borgatti, F.; Iannotta, S.; Capozi, M.; Ciullo, G.; Stierle, A. X-ray-diffraction characterization of Pt(111) surface nanopatterning induced by C-60 adsorption. *Nature Mater*. **2005**, *4*, 688-692.

[33] Orzali, T.; Forrer, D.; Sambi, M.; Vittadini, A.; Casarin, M.; Tondello, E. Temperature-dependent self-assemblies of C(60) on (1x2)-Pt(110): A STM/DFT investigation. *J. Phys. Chem. C*. **2008**, *112*, 378-390.

[34] Weckesser, J.; Barth, J. V.; Kern, K. Mobility and bonding transition of C-60 on Pd(110). *Phys. Rev. B.* 2**001**, *64*, 161403.

[35] Altman, E. I.; Colton, R. J. Interaction of C-60 with the Au(111) 23x-root-3 reconstructions. *J. Vac. Sci. & Technol. B.* **1994**, *12*, 1906-1909.

[36] Gardener, J. A.; Briggs, G. A. D.; Castell, M. R. Scanning tunneling microscopy studies of C-60 monolayers on Au(111). *Phys. Rev. B*. **2009**, *80*, 235434.

[37] Schull, G.; Berndt, R. Orientationally ordered (7x7) superstructure of C(60) on Au(111). *Phys. Rev. Lett.* **2007**, *99*, 226105.

[38] Zhang, X.; Yin, F.; Palmer, R. E.; Guo, Q. The C60/Au(111) interface at room temperature: A scanning tunnelling microscopy study. *Surf. Sci*. **2008**, *602*, 885-892.

[39] Guo, Q. Directed molecular self-assembly on metal surfaces: C_{60} molecules on the (111) surface of gold, in "Molecular self-assembly: Advances in chemistry, biology and nanotechnology". Nova Scientific Publishers. **2010**.

[40] Tang, L.; Xie, Y. C.; Guo, Q. Probing the buried C-60/Au(111) interface with atoms *J. Chem. Phys*. **2012,** *136*, 214706.

[41] Xie, Y. C.; Tang, L.; Guo, Q. Cooperative assembly of magic number C-60-Au complexes. *Phys. Rev. Lett.* **2013**, *111*, 186101.

[42] Tang, L.; Guo, Q. Orientational ordering of the second layer of C-60 molecules on Au(111). *Phys. Chem. Chem. Phys*. **2012**, *14*, 3323-3328.

[43] Xie, Y. C.; Tang, L.; Guo, Q. Underlayer growth of a nanoporous single atomic layer of gold. *J. Phys. Chem*. C. **2012**, *116*, 5103-5109.

[44] Tang, L.; Xie, Y. C.; Guo, Q. Complex orientational ordering of C-60 molecules on Au(111) *J. Chem. Phys.* 2**011**, *135*, 114702.

[45] Tang, L.; Zhang, X.; Guo, Q.; Wu, Y. N.; Wang, L. L.; Cheng, H. P. Two bonding configurations for individually adsorbed C-60 molecules on Au(111). *Phys. Rev. B.* **2010**, *82*, 125414.

[46] Tang, L.; Zhang, X.; Guo, Q. Organizing C-60 molecules on a nanostructured Au(111) surface. *Surf. Sci*. **2010**, *604*, 1310-1314.

[47] Zhang, X.; Tang, L.; Guo, Q. Low-temperature growth of C-60 monolayers on Au(111): Island orientation control with site-selective nucleation. *J. Phys. Chem. C.* **2010**, *114*, 6433-6439.

[48] Tang, L.; Zhang, X.; Guo, Q. Site-specific chemistry directed by a bifunctional nanostructured surface. *Langmuir.* **2010**, **2***6*, 4860-4864.

[49] Guo, Q.; Li, F. S. Self-assembled alkanethiol monolayers on gold surfaces: resolving the complex structure at the interface by STM. *Phys. Chem. Chem. Phys.* **2014**, *16*, 19074-19090.

[50] Gao, J.; Li, F. S.; Guo, Q. Balance of forces in self-assembled monolayers. *J. Phys. Chem. C.* **2013**, *117*, 24985-24990.

[51] Gao, J.; Li, F. S.; Guo, Q. Mixed methyl- and propyl-thiolate monolayers on a Au(111) Surface. *Langmuir.* **2013**, *29*, 11082-11086.

[52] Tang, L.; Li, F. S.; Guo, Q. Complete structural phases of self-assembled methylthiolate monolayers on Au(111). *J. Phys. Chem. C*. 2**013**, *117*, 21234.

[53] Li, F. S.; Tang, L.; Voznyy, O.; Gao, J.; Guo, Q. The striped phases of ethylthiolate monolayers on the Au(111) surface: A scanning tunneling microscopy study. *J. Chem. Phys.* **2013**, *138*, 194707.

[54] Zeng, C.; Wang, B.; Li, B.; Wang, H.; Hou, J. G. Self-assembly of one-dimensional molecular and atomic chains using striped alkanethiol structures as templates. *Appl. Phys. Lett*. **2001**, *79*, 1685-1687.

[55] Poirier, G. E.; Pylant, E. D. *Science* **1996**, *272*, 1145-1148.

[56] Li, F. S.; Tang, L.; Zhou, W. C.; Guo, Q. Formation of confined C-60 islands within octanethiol self-assembled monolayers on Au(111). *J. Phys. Chem C.* **2009**, *113*, 17899-17903.

[57] Zhang, J. L.; Zhong, S.; Zhong, J. Q.; Niu, T. C.; Hu, W. P.; Wee, A. T. S.; Chen. W. Rational design of two-dimensional molecular donor-acceptor nanostructure arrays. *Nanoscale*. **2015**, *7*, 4306-4324.

[58] Piot, L; Silly, F.; Tortech, L.; Nicolas, Y.; Blanchard, P.; Roncali, J.; Fichou, D. Long-range alignments of single fullerenes by site-selective inclusion into a double-cavity 2D open network. *J. Am. Chem. Soc.* **2009**, *131*, 12864.

[59] Zhang, H. L.; Chen, W.; Chen, L.; Huang, H.; Wang, X. S.; Yuhara, J.; Wee, A. T. S. C-60 molecular chains on a-sexithiophene nanostripes. *Small*. **2007**, *3*, 2015-2018.

[60] Wang, R.; Mao, H. Y.; Huang, H.; Qi, D. C.; Chen, W. Scanning tunneling microscopy and photoelectron spectroscopy investigation of the sexithiophene:C-60 donor-acceptor nanostructure formation on graphite. *J. Appl. Phys.* **2011**, *109*, 084307.

[61] Sedona, F.; Di. Marino, M.; Basagni, A.; Colazzo, L. Sambi, M. Structurally tunable self-assembled 2D cocrystals of C-60 and porphyrins on the Ag (110) surface. *J. Phys. Chem. C.* **2014**, *118*, 1587-1593.

[62] Wang, Y. B.; Lin, Z. Supramolecular interactions between fullerenes and porphyrins. *J. Am. Chem. Soc*. **2003**, *125*, 6072-6073.

[63] Smerdon, J. A.; Rankin, R. B.; Greeley, J. P.; Guisinger, N. P.; Guest, J. R. Chiral "pinwheel" heterojunctions self-assembled from C-60 and pentacene. *ACS Nano*. 2**013**, *7*, 3086-3094.

[64] Deering, A. L.; Kandel, S. A. Structure rearrangement of C_{70} monolayres induced by octanethiol adsorption. *Langmuir*, **2006**, *22*, 10025-10031,

TOC graphic